Momentum, Density, and Isospin dependence of the Symmetric and Asymmetric Nuclear Matter Properties.

E. N. E. van Dalen, C. Fuchs, and Amand Faessler

Institut für Theoretische Physik, Universität Tübingen,

Auf der Morgenstelle 14, D-72076 Tübingen, Germany

Abstract

Properties of symmetric and asymmetric nuclear matter have been investigated in the relativistic Dirac-Brueckner-Hartree-Fock approach based on projection techniques using the Bonn A potential. The momentum, density, and isospin dependence of the optical potentials and nucleon effective masses are studied. It turns out that the isovector optical potential depends sensitively on density and momentum, but is almost insensitive to the isospin asymmetry. Furthermore, the Dirac mass m_D^* and the nonrelativistic mass m_{NR}^* which parametrizes the energy dependence of the single particle spectrum, are both determined from relativistic Dirac-Brueckner-Hartree-Fock calculations. The nonrelativistic mass shows a characteristic peak structure at momenta slightly above the Fermi momentum k_F. The relativistic Dirac mass shows a proton-neutron mass splitting of $m_{D,n}^* < m_{D,p}^*$ in isospin asymmetric nuclear matter. However, the nonrelativistic mass has a reversed mass splitting $m_{NR,n}^* > m_{NR,p}^*$ which is in agreement with the results from nonrelativistic calculations.

PACS numbers: 21.65.+f,21.60.-n,21.30.-x,24.10.Cn

I.   INTRODUCTION

A highly discussed topic is the isovector dependence of the nuclear force. This isovector dependence of the nuclear force can be found in the symmetry energy, the proton-neutron mass splitting, and the isovector optical potential.

The behavior of the nuclear symmetry energy at high densities is an important issue in astrophysics, because the proton fraction inside a neutron star is strongly dependent on the nuclear symmetry energy. Therefore, a stiff nuclear symmetry energy leads to a relative proton-rich neutron star, whereas a soft one results in a neutron star with only a very small proton fraction. The proton-richness of a neutron star has consequences for the chemical composition and cooling mechanism of protoneutron stars [1, 2, 3], mass-radius correlations [4, 5], critical densities for kaon condensation in dense stellar matter [6, 7], and the possibility of a mixed quark-hadron phase in neutron stars [8]. For example, consider the crucial role of the proton-richness in the thermal evolution of neutron stars. In fact, if the proton fraction in the core of a neutron star is above a critical value, the so-called direct Urca processes can occur [1, 2, 3]. If they occur, the direct Urca processes will enhance the neutrino emission and neutron star cooling rate by a large factor compared to the standard cooling scenario, in which the relatively slow modified Urca and two-body neutrino bremsstrahlung processes play a role [9, 10, 11, 12, 13].

The interest for the isospin dependence of the nuclear forces at its extremes is of recent date, because data for neutron-rich nuclei were rather scarce in the past. However, the forthcoming new generation of radioactive beam facilities, e.g. the future GSI facility FAIR in Germany, the Rare Isotope Accelerator planned in the United States of America or SPIRAL2 at GANIL/France, will produce huge amounts of new data for neutron-rich nuclei.

Currently, the isovector dependence of the nuclear force has been investigated in the heavy ion experiments. For a recent review see [14]. The observables in these experiments are the n/p flow [15, 16], isospin tracing [17], isoscaling of intermediate mass fragments (IMF) [18], and π^+/π^- production [19, 20]. Heavy ion reactions have the advantage that they allow to test the nuclear forces at supra-normal densities since in intermediate energy reactions compressions of two to three times nuclear saturation density n_0 are reached. However, the asymmetry of the colliding systems is moderate and therefore the isospin effects on the

corresponding observables are generally moderate as well. The interpretation of the various data by transport calculations supports at present a value of the symmetry energy around $E_{sym} \sim 32$ MeV at saturation density with a not too soft increase with density.

However, the theoretical predictions for the isospin dependence of nuclear interactions are still very different. The symmetry energy in relativistic Dirac-Brueckner-Hartree-Fock (DBHF) calculations is found to be significantly stiffer than in non-relativistic Brueckner-Hartree-Fock (BHF) approaches [21]. At moderate densities the DBHF dependence of E_{sym} is qualitatively similar to density dependent relativistic mean-field parametrizations using $a_4 = 32 - 34$ MeV [22]. However, the density dependence of E_{sym} is generally more complex than in RMF theory. In particular at high densities E_{sym} shows a non-linear and more pronounced increase. In addition, the present predictions for the isospin dependence of the effective masses differ substantially [14]. BHF calculations [23, 24, 25, 26], a nonrelativistic *ab initio* approach, predict a proton-neutron mass splitting of $m^*_{NR,n} > m^*_{NR,p}$ in isospin asymmetric nuclear matter. This prediction stands in contrast to the one from relativistic mean-field (RMF) theory. When only a vector isovector ρ-meson is included in RMF theory, Dirac phenomenology predicts equal masses $m^*_{D,n} = m^*_{D,p}$. The inclusion of the scalar isovector δ-meson, i.e. $\rho + \delta$, in this theory leads even to $m^*_{D,n} < m^*_{D,p}$ [14, 27]. The nonrelativistic mass derived from RMF theory shows the same behavior as its Dirac mass, namely $m^*_{NR,n} < m^*_{NR,p}$ [14]. The various Skyrme forces give opposite predictions for the neutron-proton mass splitting and also for the energy slope of the isovector optical potential.

Relativistic *ab initio* calculations which are based on realistic nucleon-nucleon interactions, such as the DBHF approach, are the proper tool to answer these questions. Therefore, in the present paper, which is an extension of the work done in Ref. [28], the DBHF approach based on projection techniques is used to determine properties of symmetric and asymmetric nuclear matter. The momentum, density, and isospin dependence of these properties are investigated. The DBHF results for the symmetry energy are compared to results from some phenomenological approaches. The application of the DBHF approach allows one to determine the Dirac mass and the nonrelativistic mass from the same approach. The results are compared to nonrelativistic BHF and RMF approaches. In addition, the isovector optical nucleon potential, which is of importance for transport models in relation with the collisions of radioactive nuclei, is investigated.

The present paper is organized as follows. In Sec. II we give a short description of the

relativistic DBHF approach. In Sec. III, we survey the different definitions and physical concepts of the effective nucleon mass. In Sec. IV, we present the results derived from the DBHF approach, which is based on projection techniques, in isospin symmetric and asymmetric nuclear matter and investigate the momentum, density, and isospin dependence of the nucleon effective masses and the optical potentials. Section V contains a summary and the conclusions of our work.

II. RELATIVISTIC BRUECKNER APPROACH

In the relativistic Brueckner approach nucleons are dressed inside nuclear matter as a consequence of their two-body interactions with the surrounding particles. Starting point is the in-medium interaction, i.e. the T matrix. It is treated in the ladder approximation of the relativistic Bethe-Salpeter (BS) equation

$$T = V + i \int VQGGT, \tag{1}$$

where V denotes the bare nucleon-nucleon interaction and G the intermediate off-shell nucleon. The Pauli operator Q accounts for the Pauli principle preventing the scattering to occupied states. The Green's function G describes the propagation of dressed nucleons in the medium and fulfills the Dyson equation

$$G = G_0 + G_0 \Sigma G. \tag{2}$$

G_0 denotes the free nucleon propagator, whereas the influence of the nuclear medium is expressed by the self-energy Σ. In the Brueckner formalism this self-energy Σ is determined by summing up the interactions with all the nucleons inside the Fermi sea F in Hartree-Fock approximation

$$\Sigma = -i \int_F (Tr[GT] - GT). \tag{3}$$

The coupled set of Eqs. (1)-(3) represents a self-consistency problem and has to be solved by iteration. The self-energy consists of scalar Σ_s and vector $\Sigma^\mu = (\Sigma_\mathrm{o}, \mathbf{k}\,\Sigma_\mathrm{v})$ components

$$\Sigma(k, k_\mathrm{F}) = \Sigma_\mathrm{s}(k, k_\mathrm{F}) - \gamma_0\,\Sigma_\mathrm{o}(k, k_\mathrm{F}) + \boldsymbol{\gamma} \cdot \mathbf{k}\,\Sigma_\mathrm{v}(k, k_\mathrm{F}). \tag{4}$$

The DBHF approach is the proper tool to investigate the properties of nuclear matter, but results from DBHF calculations are still controversial. These results depend strongly

on approximation schemes and techniques used to determine the Lorentz and the isovector structure of the nucleon self-energy. In the present paper, the projection technique method is used, which requires the knowledge of the Lorentz structure of the T-matrix in (3). For this purpose the T-matrix has to be projected onto covariant amplitudes. Hence, the scalar and vector components of the self-energies can directly be determined from the projection onto Lorentz invariant amplitudes. We use the subtracted T-matrix representation scheme for the projection method described in detail in [29, 30]. Projection techniques are rather complicated, but are accurate. For example, they have been used in Refs. [29, 31, 32].

Another frequently used approach, which is called fit method in the following, was originally proposed by Brockmann and Machleidt [33]. In this approach, one extracts the scalar and vector self-energy components directly from the single particle potential. Hence, mean values for the self-energy components are obtained where the explicit momentum-dependence has already been averaged out. In symmetric nuclear matter this method is relatively reliable. However, the extrapolation to asymmetric matter introduces two new parameters in order to fix the isovector dependencies of the self-energy components. This makes this procedure ambiguous [34].

The quantity which characterizes the isospin dependence of the nuclear equation of state (EoS) is the symmetry energy. The energy functional of nuclear matter can be expanded in terms of the asymmetry parameter $\beta = (n_n - n_p)/n_B$ (n_n and n_p are the neutron and proton densities, respectively) which leads to a parabolic dependence on β

$$E(n_B, \beta) = E(n_B) + E_{sym}(n_B)\beta^2 + \mathcal{O}(\beta^4). \tag{5}$$

In Fig. 1 the symmetry energy from the DBHF approach using the Bonn A potential [30] is compared to the phenomenological models NL3, DD, and D^{3}C. NL3 is a nonlinear parametrization [35] that is widely used in RMF calculations. The DD model is based on a Lagrangian density of standard relativistic mean-field models with density dependent meson-nucleon coupling vertices. The D^{3}C model, in addition, introduces couplings of the meson fields to derivative nucleon densities in the Lagrangian density [36]. The NL3 model has the stiffest EoS and the symmetry energy rises almost linearly with the density. In contrast, the DD and D^{3}C model exhibit a considerable flattening. The DBHF results are more complex and have a nonlinear increase at high densities. At high densities the symmetry energy lies between the stiff NL3 model and the soft DD and D^{3}C models. It is worth noting
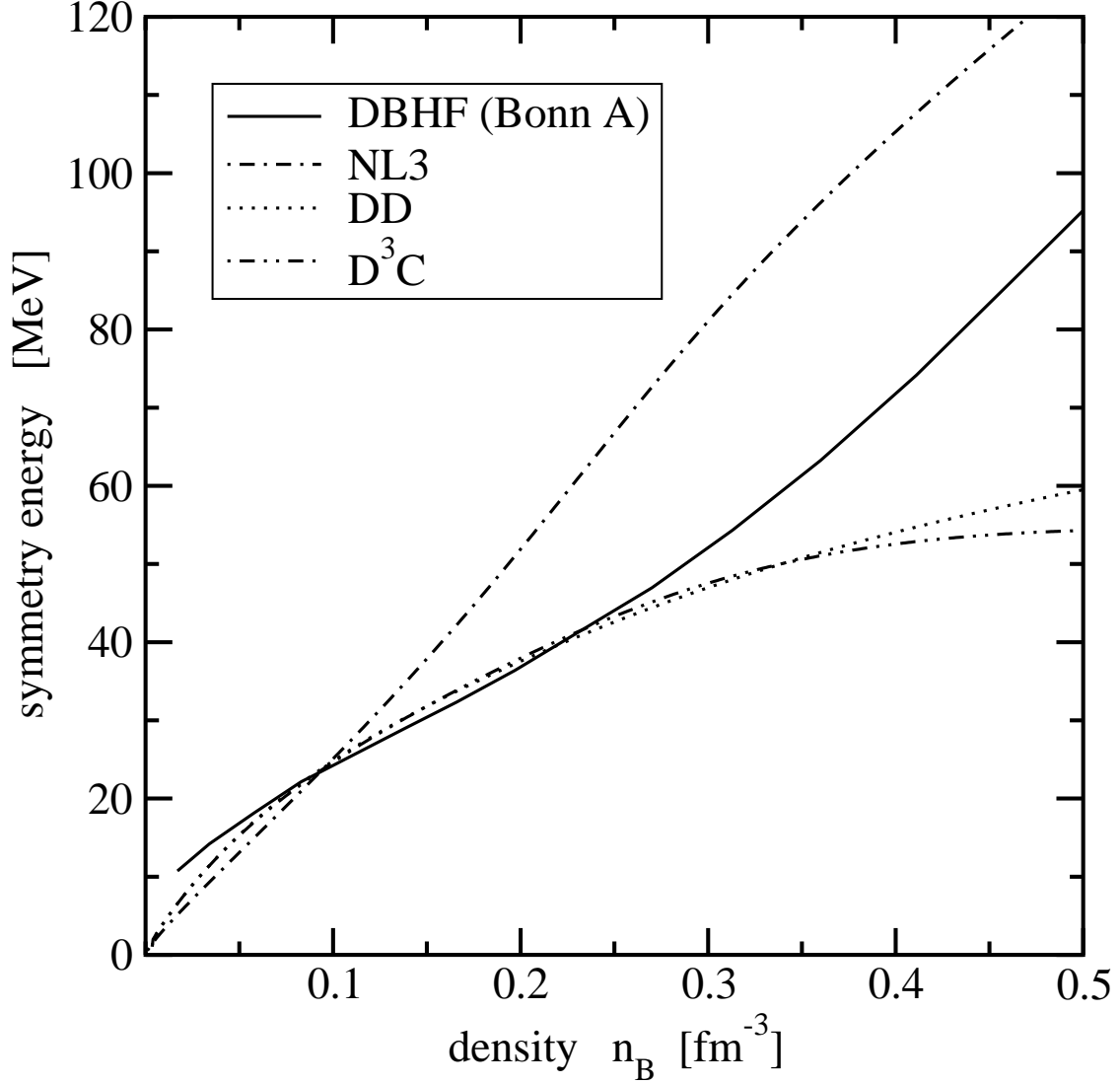
FIG. 1: Symmetry energy as a function of the nucleon density n_B. The DBHF result is compared to various phenomenological RMF models.

that the symmetry energies in the models are rather similar at a density near 0.1 fm^{-3}. In phenomenological models the symmetry energy is constrained by the skin thickness of heavy nuclei which, due to surface effects, seems to fix the symmetry energy at an average density of about 0.1 fm^{-3}. That the DBHF result coincides at this density with RMF phenomenology shows that the low density behavior of the microscopic calculation is in agreement with the constraints from finite nuclei.

III. EFFECTIVE MASSES

In the field of nuclear physics, the introduction of an effective mass is a common concept to characterize the quasi-particle properties of a particle inside a strongly interacting medium. A well established fact is that the effective nucleon mass in nuclear matter or finite nuclei deviates substantially from its vacuum value [37, 38, 39]. However, the expression of an effective nucleon mass has been used to denote different quantities, which are sometimes even mixed up: the nonrelativistic effective mass m^*_{NR} and the relativistic Dirac mass m^*_D. Although these different definitions of the effective mass are related, they are based on completely different physical concepts. Hence, one has to be careful when relativistic and nonrelativistic approaches are compared on the basis of effective masses. Whereas the nonrelativistic mass m^*_{NR} can be determined from both, relativistic as well as nonrelativistic approaches, the Dirac mass is a genuine relativistic quantity. Therefore, the definitions of the relativistic Dirac mass and of the nonrelativistic mass are given below.

A. Dirac Mass

The relativistic Dirac mass is defined through the scalar part of the nucleon self-energy in the Dirac field equation which is absorbed into the effective mass

$$m^*_D(k, k_\mathrm{F}) = \frac{M + \Re\Sigma_s(k, k_\mathrm{F})}{1 + \Re\Sigma_\mathrm{v}(k, k_\mathrm{F})} \quad , \tag{6}$$

where Σ_s and Σ_v are, respectively, the scalar part and the spatial vector part of the nucleon self-energy (4). The Dirac mass accounts for medium effects through the scalar part of the self-energy. The correction through the spatial vector part of the self-energy is generally small [29, 30, 31]. Furthermore, the Dirac mass is a smooth function of the momentum.

B. Nonrelativistic Mass

The effective nonrelativistic mass, which is usually considered in order to characterize the quasi-particle properties of the nucleon within nonrelativistic frameworks, is defined as

$$m^*_{NR} = |\mathbf{k}|[dE/d|\mathbf{k}|]^{-1} \quad , \tag{7}$$

where E is the quasi-particle's energy and $\mathbf{k}$ its momentum. When evaluated at $k = k_F$, Eq.(7) yields the Landau mass $m^*_L = M(1 + f_1/3)$ related to the f_1 Landau parameter of a

Fermi liquid [14, 40]. In the quasi-particle approximation, i.e. the zero width limit of the in-medium spectral function, the quantities E and m_{NR}^* are connected by the dispersion relation

$$E = \frac{\mathbf{k}^2}{2M} + \Re U(|\mathbf{k}|, k_{\mathrm{F}}) \quad . \tag{8}$$

Therefore, equations (7) and (8) yield the following expression for the nonrelativistic effective mass

$$m_{NR}^* = \left[\frac{1}{M} + \frac{1}{|\mathbf{k}|} \frac{d}{d|\mathbf{k}|} \Re U \right]^{-1} \quad . \tag{9}$$

In a relativistic framework m_{NR}^* is then obtained from the corresponding Schroedinger equivalent single particle potential

$$U(|\mathbf{k}|, k_{\mathrm{F}}) = \Sigma_{\mathrm{s}} - \frac{1}{M} \left(E\Sigma_{\mathrm{o}} - \mathbf{k}^2 \Sigma_{\mathrm{v}} \right) + \frac{\Sigma_{\mathrm{s}}^2 - \Sigma_{\mu}^2}{2M} \quad . \tag{10}$$

An alternative would be to derive the effective mass from Eq. (7) via the relativistic single particle energy

$$E = (1 + \Re\Sigma_{\mathrm{v}}) \sqrt{\mathbf{k}^2 + m_D^{*2}} - \Re\Sigma_{\mathrm{o}}. \tag{11}$$

However, the single particle energy contains relativistic corrections to the kinetic energy. These kind of corrections should be avoided in a comparison to nonrelativistic approaches. Hence, the effective mass should be based on the Schroedinger equivalent potential (10) [40].

The nonrelativistic effective mass parametrizes the momentum dependence of the single particle potential. Therefore, it is a measure of the nonlocality of the single particle potential U. The nonlocality of U can be due to nonlocalities in space or in time. The spatial nonlocalities result in a momentum dependence, whereas nonlocalities in time result in an energy dependence. In order to separate both effects, one has to distinguish between the so-called k-mass, which is obtained from Eq. (9) at *fixed* energy, and the E-mass, which is given by the derivative of U with respect to the energy at *fixed* momentum [40]. Knowledge of the off-shell behavior of the single particle potential U is needed for a rigorous distinction between these two masses. The spatial nonlocalities of U are mainly generated by exchange Fock terms [24, 25] and the resulting k-mass is a smooth function of the momentum. Nonlocalities in time are generated by Brueckner ladder correlations due to the scattering to intermediate off-shell states. These correlations are mainly short-range correlations which

8

generate a strong momentum dependence with a characteristic enhancement of the E-mass slightly above the Fermi surface [24, 25, 39, 40]. The effective nonrelativistic mass defined by Eqs. (7) and (9) is given by the product of k-mass and E-mass [40]. Thus, it contains both, nonlocalities in space and time. Therefore, it should also show a typical peak structure around k_F. This peak structure reflects - as a model independent result - the increase of the level density due to the vanishing imaginary part of the optical potential at k_F, which for example is seen in shell model calculations [38, 39, 40]. However, one should account for correlations beyond mean-field or Hartree-Fock in order to reproduce this behavior.

IV.   RESULTS AND DISCUSSION

In the following we present the results for the properties of symmetric and asymmetric nuclear matter obtained from the DBHF approach based on projection techniques. The nucleon-nucleon potential used is Bonn A. However, the presented results and the following discussion do not strongly depend on the particular choice of the interaction.

A.   Symmetric Nuclear Matter

In Fig. 2 the nucleon optical potential, which is closely related to the nonrelativistic mass, is plotted as a function of the momentum $k = |\mathbf{k}|$ at different Fermi momenta of $k_F = 1.07$, 1.35, and 1.7 fm^{-1} which corresponds to nuclear densities $n_B = 4k_F^3/6\pi^2 = 0.5n_0$, n_0, and $2n_0$ with $n_0 = 0.166$ fm^{-3}. The depth of the nucleon optical potential at k=0 is larger at higher densities. Furthermore, the potential increases with momentum at all three densities. However, the slope of the optical potential is steeper at higher densities.

In Fig. 3 the nonrelativistic effective mass and the Dirac mass are shown as a function of momentum k at nuclear densities $n_B = 4k_F^3/6\pi^2 = 0.5n_0$, n_0, and $2n_0$. Both, Dirac and nonrelativistic mass, decrease in average with increasing nuclear density. The decrease of the nonrelativistic mass could already be expected on the basis of the slope of the optical potential in Fig. 2. The projection method reproduces a pronounced peak of the nonrelativistic mass slightly above the Fermi momentum k_F, as it is also seen in nonrelativistic BHF calculations [40]. This peak is shifted to higher momenta and slightly broadened with increasing density. On the other hand, the Dirac mass is a smooth function of k with only
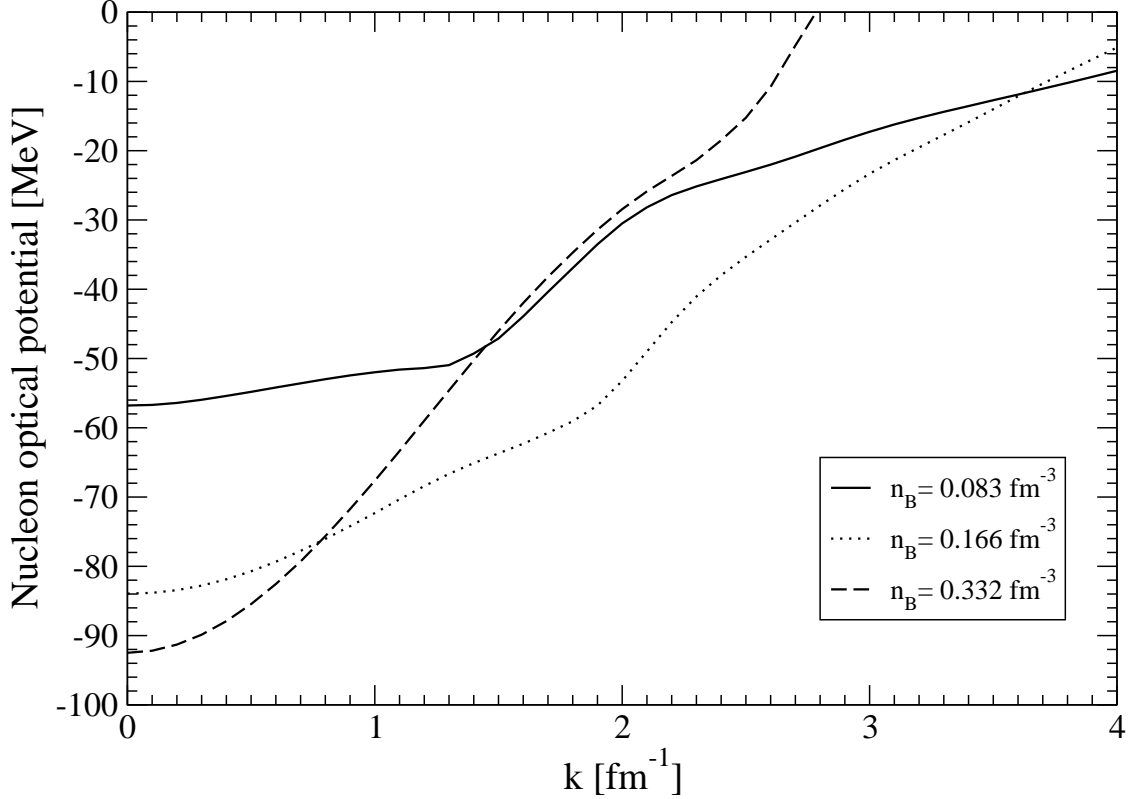
FIG. 2: The nucleon optical potential in isospin symmetric nuclear matter as a function of the momentum $k = |\mathbf{k}|$ at different densities.

a moderate momentum dependence. This behavior is in agreement with the "reference spectrum approximation" used in the self-consistency scheme of the DBHF approach [30].

The nonrelativistic mass, plotted in Fig. 4, is derived from Eq. (7) via the single particle energy instead of from Eq. (10) via the potential. The results are very similar to the ones in Fig. 3. Again the pronounced peak of the nonrelativistic mass slightly above the Fermi momentum k_F is reproduced, although it is more broadened and as a result it is more a broad bump at high densities. The important difference is the strong increase of the effective nonrelativistic mass at high momentum compared to the nonrelativistic mass extracted from the potential. Relativistic corrections to the kinetic energy are responsible for this high momentum behavior. Hence, a comparison to nonrelativistic approaches should be based on the Schroedinger equivalent potential (10) [40].

Relativistically, the single particle potential and the corresponding peak structure of the nonrelativistic mass are the result of subtle cancellation effects of the scalar and vector self-
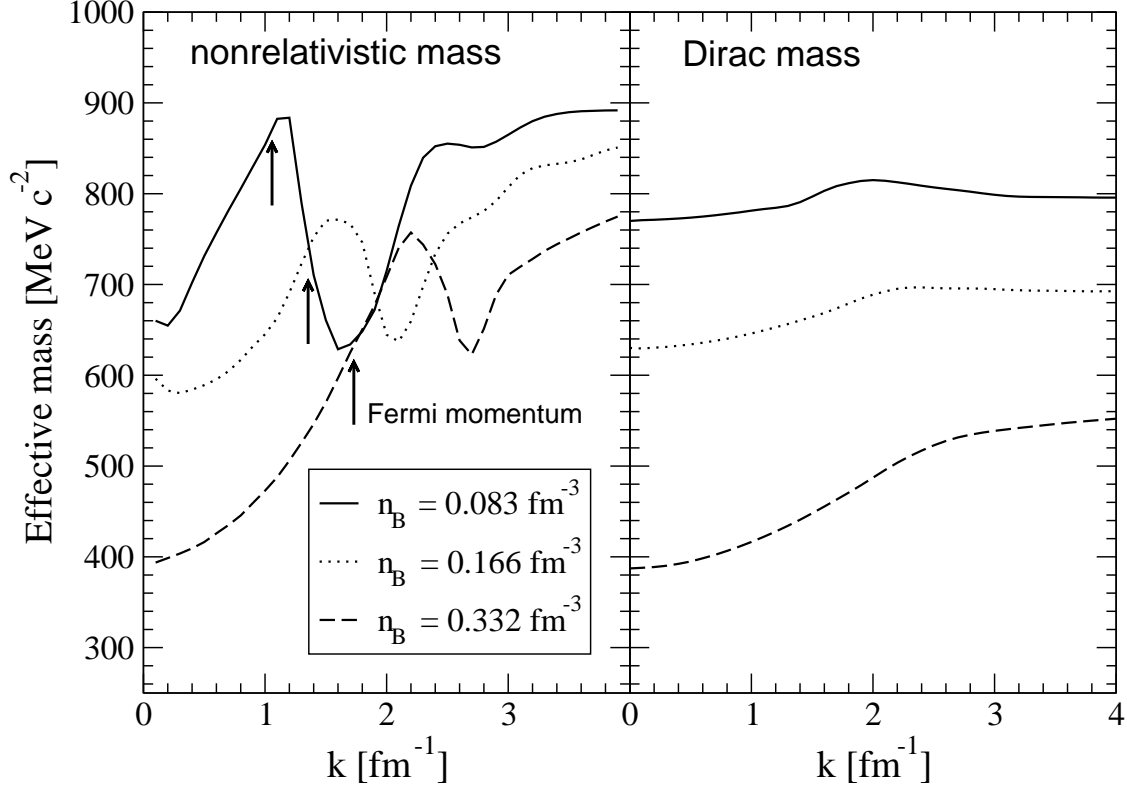
FIG. 3: The effective mass in isospin symmetric nuclear matter as a function of the momentum $k = |\mathbf{k}|$ at different densities.

energy components. Therefore, this requires a very precise method in order to determine variations of the self-energies Σ which are small compared to their absolute scale. The applied projection techniques are the adequate tool for this purpose. Less precise methods yield only a small enhancement, i.e. a broad bump around the Fermi momentum k_F [31, 40]. The extraction of mean scalar and vector self-energy components from a fit to the single particle potential, is not able to resolve such a structure at all.

The density dependence of the two effective masses is compared in Fig. 5. Both, the nonrelativistic (Landau) and the Dirac mass are determined at $k = |\mathbf{k}| = k_F$ and shown as a function of k_F. The Dirac mass decreases continously with increasing Fermi momentum k_F. Initially, the Landau mass decreases with increasing Fermi momentum k_F like the Dirac mass. However, it starts to rise again at high values of the Fermi momentum k_F. In addition, also results from nonrelativistic BHF calculations [41], which are based on the same Bonn A interaction, are plotted. The agreement between the nonrelativistic and the
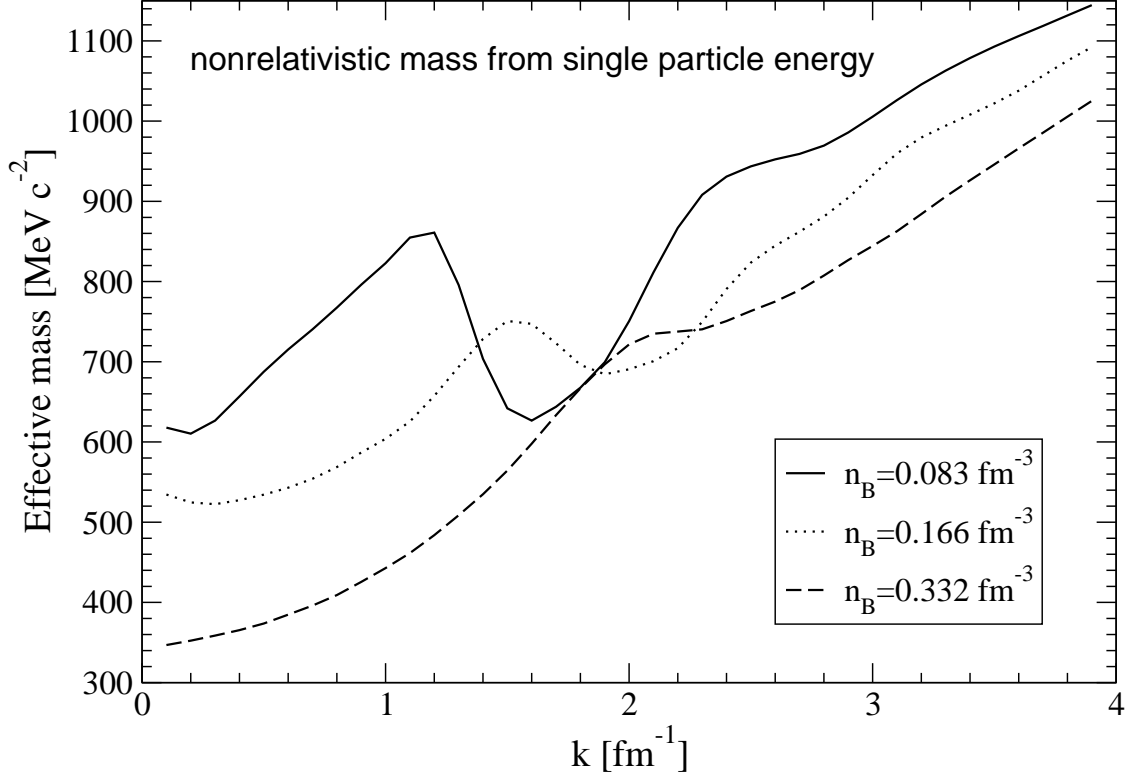
FIG. 4: The nonrelativistic effective mass in isospin symmetric nuclear matter extracted from the single particle energy (7) as a function of the momentum $k = |\mathbf{k}|$ at different densities.

relativistic Brueckner approach is quite good. This demonstrates that the often discussed difference between effective masses obtained in the various approaches is mainly due to different definitions, i.e. nonrelativistic mass versus Dirac mass. If the same quantity is determined from DBHF and BHF, this leads to results which are very close. Furthermore, also results from the NL3, DD, and D^{3}C model are shown. They qualitatively show the same behavior as the Brueckner approaches, i.e. the Landau mass and the Dirac mass decrease with increasing Fermi momentum. However, the Landau mass starts to rise again at high values of the Fermi momentum $k_{\rm F}$. But quantitatively these masses are lower compared to the ones in the Brueckner approaches.

B. Asymmetric Nuclear Matter

In Fig. 6 the neutron and proton optical potentials in isospin asymmetric nuclear matter are plotted as a function of the momentum $k = |\mathbf{k}|$ for various values of the asymmetry
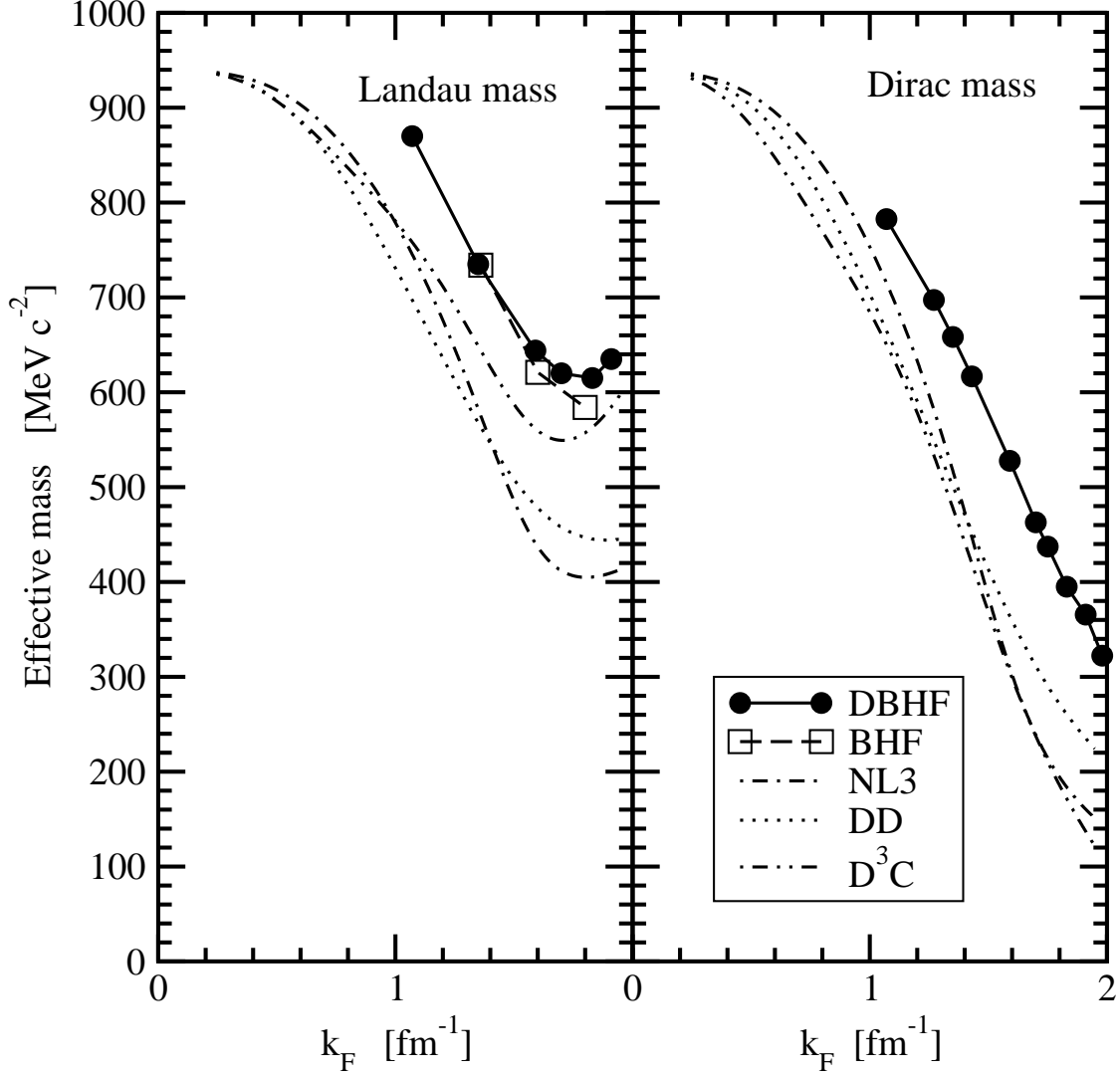
FIG. 5: The effective mass in isospin symmetric nuclear matter at $k = |\mathbf{k}| = k_F$ as a function of the Fermi momentum k_F for the various models.

parameter $\beta = (n_n - n_p)/n_B$ at fixed nuclear density $n_B = 0.166$ fm^{-3}. The proton optical potential decreases with increasing asymmetry. The neutron optical potential, in contrast, shows an opposite behavior. In addition, the steepness of the neutron optical potential decreases with increasing asymmetry parameter β, whereas the opposite behavior is found in the proton case.

The isovector optical potential

$$U_{iso} = \frac{U_n - U_p}{2\beta} \qquad (12)$$

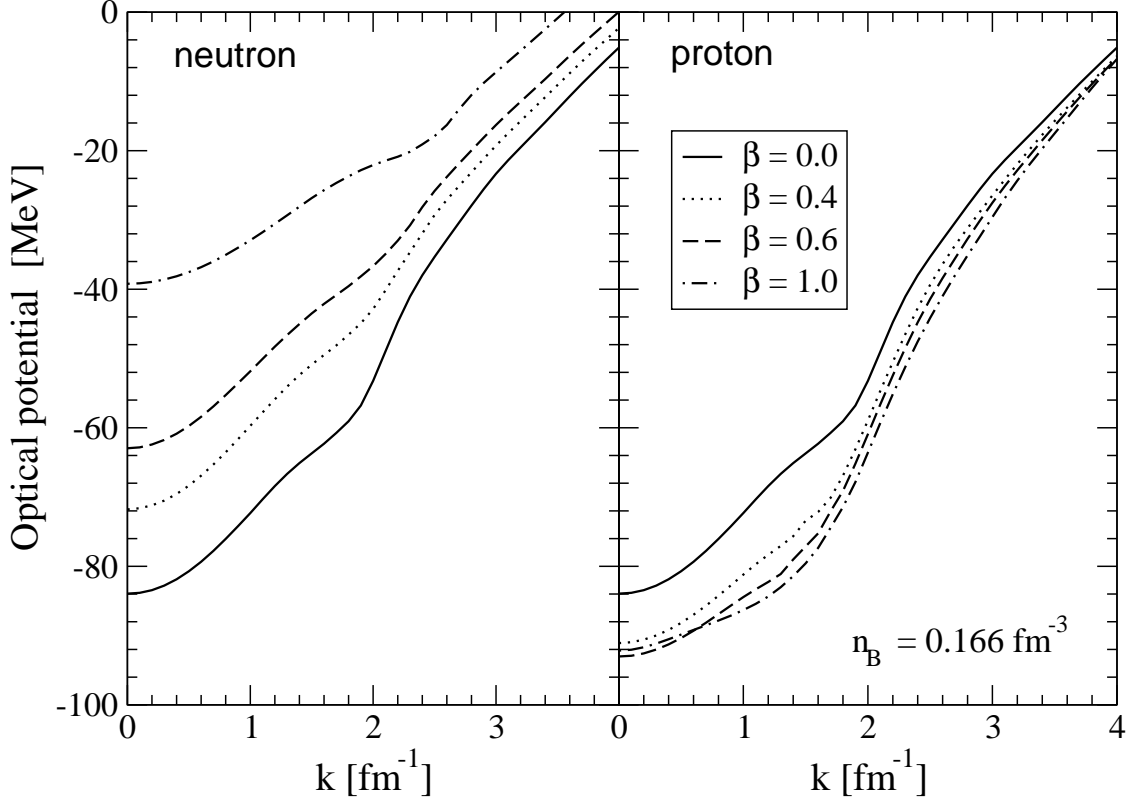can be obtained from the neutron and proton optical potential. In Fig. 7 the isovector optical

FIG. 6: The neutron and proton optical potential in isospin asymmetric nuclear matter as a function of the momentum $k = |\mathbf{k}|$ at different densities.

potential is displayed as a function of momentum k for three densities and several isospin asymmetries. It is seen that the isovector optical potential depends strongly on density and momentum. The optical potential in neutron-rich matter stays roughly constant up to a momentum between 1 to 2 fm^{-1}, depending on the density, and then decreases strongly with increasing momentum. Fig. 7 shows that the isovector optical potential is almost independent of the asymmetry parameter β. The optical isovector potential at nuclear density $n_B = 0.166$ fm^{-3} at $k = 0$ is in good agreement with the empirical value of 22 - 34 MeV [16].

Fig. (8) compares the predictions from our DBHF calculation to the nonrelativistic BHF [26] and to the phenomenological Gogny [42] and Skyrme [43] forces and a relativistic $T - \rho$ approximation [44] based on empirical relativistic NN amplitudes [45]. Our results are in good agreement with the nonrelativistic BHF results of Ref. [26], except for the negative sign of the potential at high momenta in their work. In addition, at large momenta our
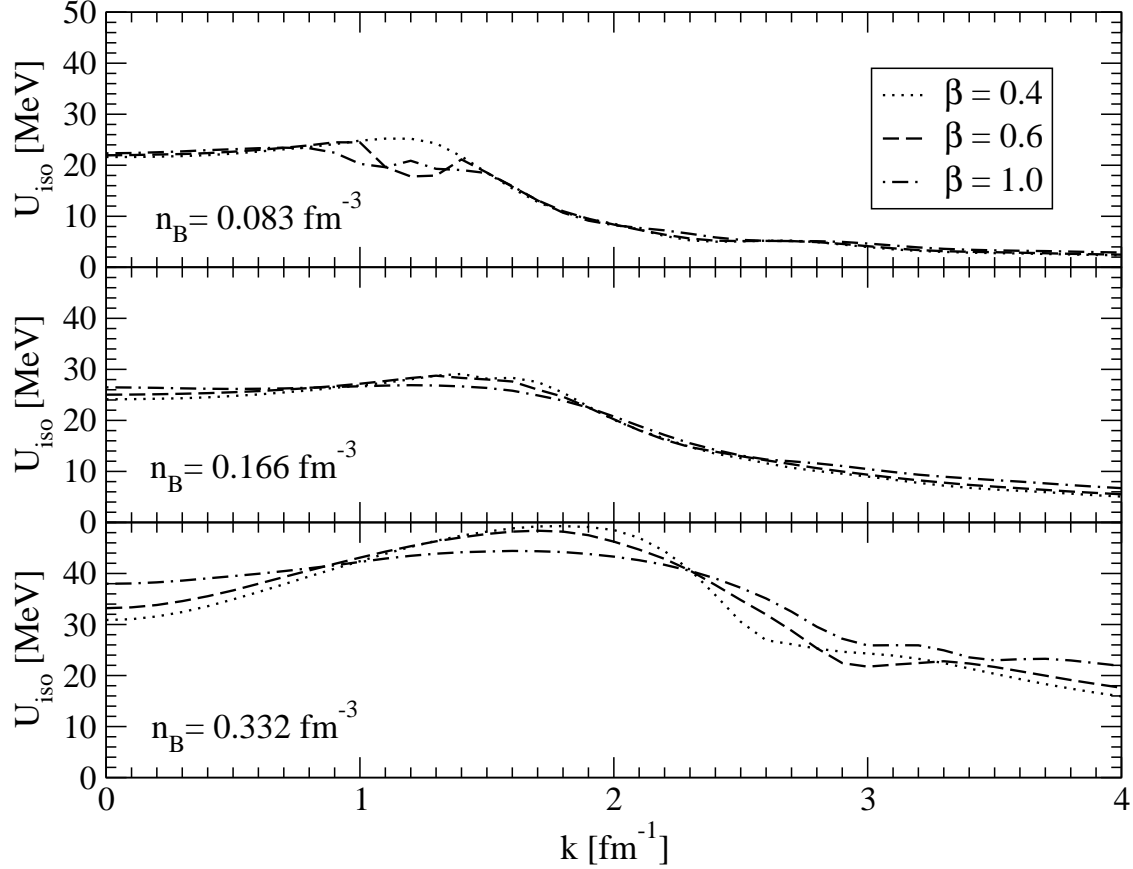
14

FIG. 7: The isovector optical potential as a function of momentum k for three densities and several isospin asymmetries.

DBHF calculation agrees with the tree-level results of [44]. This is to be expected since Pauli blocking of intermediate states in the Bethe-Salpeter equation play then a less important role. First order medium effects such as a density of the effective mass are included in both approaches, in [44] within the framework of RMF theory.

While the dependence of U_{iso} on the asymmetry parameter β is found to be weak, the predicted energy and density dependences are quite different, in particular between the microscopic and the phenomenological approaches. In mean field models, i.e., assuming momentum independent self-energy components, the energy dependence of U_{iso} is linear, i.e. quadratic in momentum. Relativisitc mean field models show throughout a positive slope [14] while Skyrme functionals can have positive slopes, e.g. some of the recent Skyrme-Lyon parameterisations [43] (SkLya), or negative ones (SkM*). In the former cases this leads to a continously increasing optical isovector potential. SkM* decreases, however, with a much
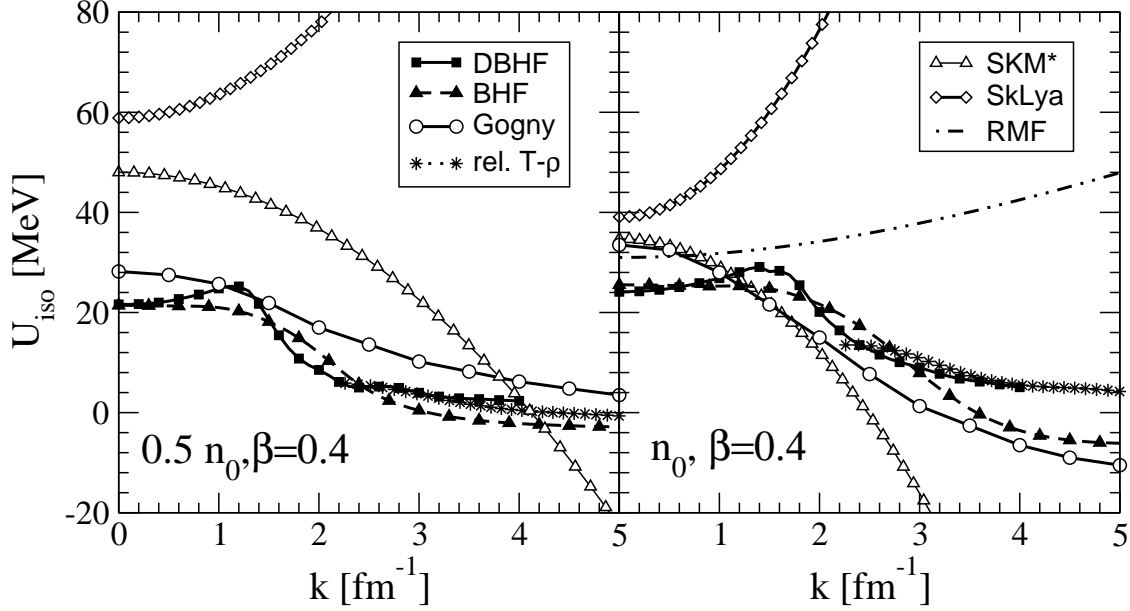
FIG. 8: The isovector optical potentials from the various models in asymmetric nuclear matter ($\beta = 0.4$) as a function of momentum k at $n = 0.5n_0$ and n_0. The isovector optical potential from our DBHF approach is compared to the ones from the nonrelativistic BHF approach [26], the phenomenological RMF [20], Gogny [42] and Skyrme [43] forces and from a relativistic $T - \rho$ approximation [44].

stronger slope than the microscopic approaches which tend to saturate at high momenta. Qualitatively such a behavior is reproduced by the Gogny force. In the DBHF case the decrease is caused by a pronounced explicit momentum dependence of the scalar and vector self-energy components.

However, the energy dependence of U_{iso} is very little constrained by data. The old analysis of Lane [46] is consistent with a decreasing potential as predicted by DBHF/BHF, while more recent analyses based on Dirac phenomenology [47] come to the opposite conclusions. Certainly more experimental efforts are necessary to clarify this question.

In Fig. 9 the neutron nonrelativistic and Dirac mass are plotted for various values of the asymmetry parameter β at nuclear density $n_B = 0.166$ fm^{-3}. An increase of β enhances the neutron density and has for the density of states the same effect as an increase of the density in symmetric matter. Therefore, a pronounced peak of the nonrelativistic mass slightly above $k_{\mathrm{F}n}$ is observed.
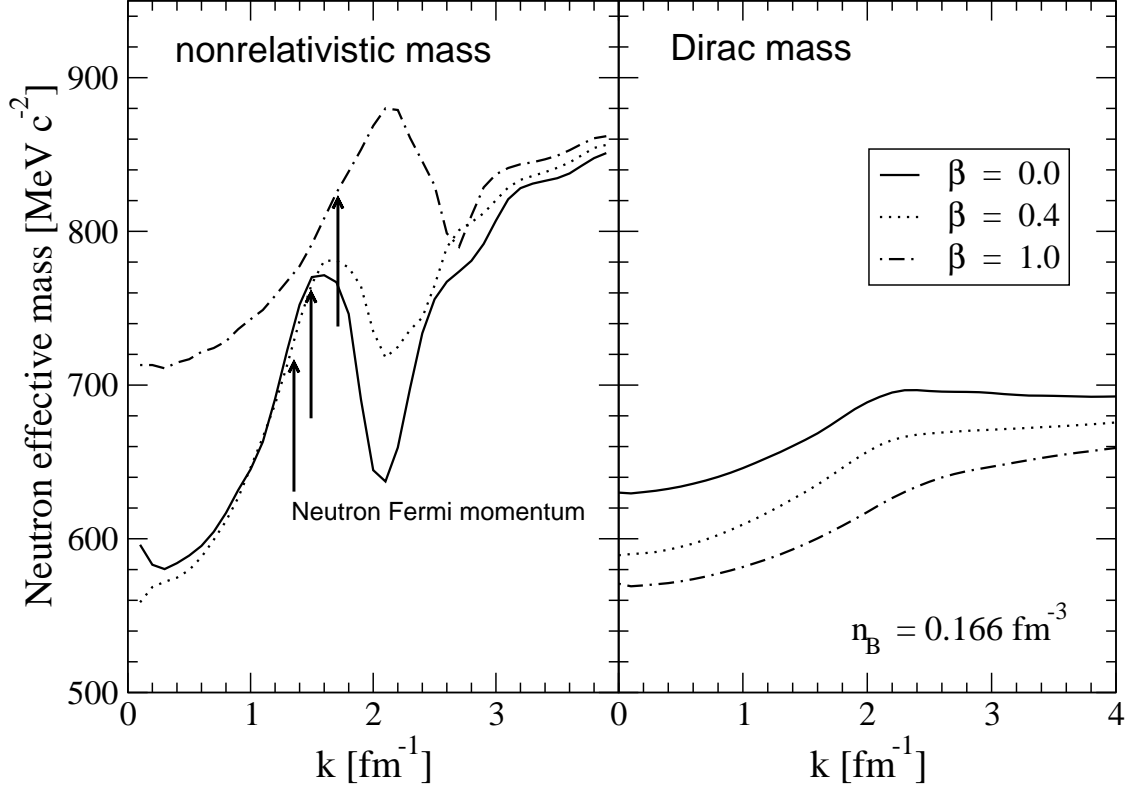
FIG. 9: Neutron effective mass as a function of the momentum $k = |\mathbf{k}|$ for various values of the asymmetry parameter β at fixed nuclear density $n_B = 0.166$ fm^{-3}.

Another interesting issue is the proton-neutron mass splitting in isospin asymmetric nuclear matter. In Fig. 10 the neutron and proton effective mass are compared for $\beta = 1$, i.e. neutron matter. Our DBHF calculations based on projection techniques predict a mass splitting of $m^*_{D,n} < m^*_{D,p}$ in isospin asymmetric nuclear matter. However, the predicted mass splitting based on the fit method is $m^*_{D,n} > m^*_{D,p}$ [48, 49]. In the fit method, the mean values for the self-energy components are obtained where the explicit momentum-dependence has already been averaged out. In symmetric nuclear matter this method is relatively reliable. However, the extrapolation to asymmetric matter introduces two new parameters in order to fix the isovector dependencies of the self-energy components. This makes the fit procedure ambiguous [34]. Other DBHF calculations based on projection techniques predict a mass splitting of $m^*_{D,n} < m^*_{D,p}$ in isospin asymmetric nuclear matter [30, 34, 50] in agreement with our results. Although the relativistic Dirac mass derived from the DBHF approach based on projection techniques has a proton-neutron mass splitting of $m^*_{D,n} < m^*_{D,p}$, as can
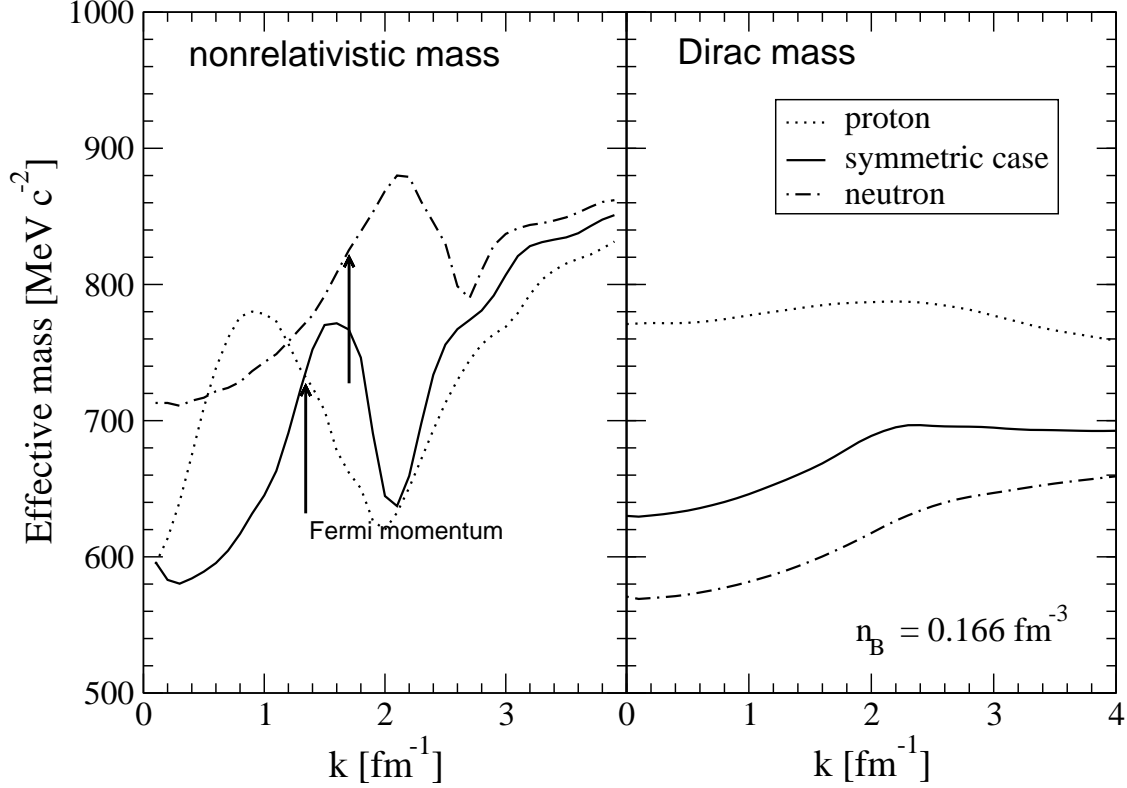
FIG. 10: Neutron and proton effective mass as a function of the momentum $k = |\mathbf{k}|$ for a value of the asymmetry parameter $\beta = 1$ at fixed nuclear density $n_B = 0.166$ fm^{-3}. In addition, the effective mass in symmetric nuclear matter is given.

be seen from Fig. 10, the nonrelativistic mass derived from the DBHF approach shows the opposite behavior, except around the peak slightly above the proton Fermi momentum k_{Fp}. This opposite behavior to the relativistic Dirac mass, i.e. $m^*_{NR,n} > m^*_{NR,p}$, is in agreement with the results from nonrelativistic BHF calculations [23, 24, 25]. This opposite behavior between the Dirac mass splitting and the nonrelativistic mass splitting is not surprising, since these masses are based on completely different physical concepts. The nonrelativistic mass parameterizes the momentum dependence of the single particle potential. It is the result of a quadratic parameterization of the single particle spectrum. On the other hand, the relativistic Dirac mass is defined through the scalar part of the nucleon self-energy in the Dirac field equation which is absorbed into the effective mass (6). In Fig. 11 the neutron nonrelativistic and the neutron Dirac mass in symmetric nuclear matter and in pure neutron matter are plotted at nuclear densities $n_B = 0.083$ fm^{-3} and $n_B = 0.166$ fm^{-3}.
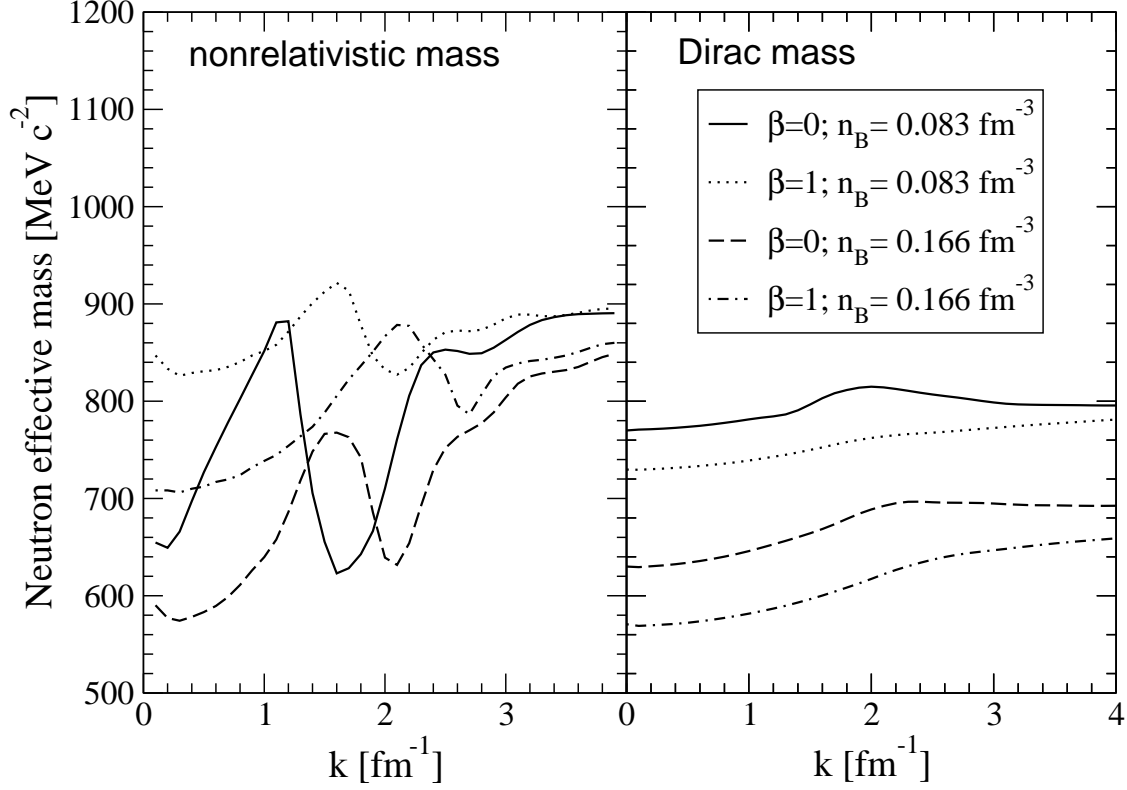
FIG. 11: Neutron effective mass in symmetric nuclear matter and in pure neutron matter as a function of the momentum $k = |\mathbf{k}|$ at different nuclear densities.

The difference between the two masses is reduced as the density gets lower, if one excludes the momentum region at the peak structure of the nonrelativistic mass. This peak structure reflects the increase of the level density due to the vanishing imaginary part of the optical potential at k_F. In addition, with decreasing density the neutron Dirac mass difference in symmetric nuclear and in pure matter gets smaller, i.e. the proton-neutron mass splitting decreases. The same picture can be observed for the nonrelativistic mass, if one does not consider the peak structure of the nonrelativistic mass.

A demonstration of the influence of the explicit momentum dependence of the DBHF self-energy is shown in Fig. 12. In RMF theory the relativistic Dirac mass and the vector self-energy are momentum independent. The nonrelativistic mass is determined from the RMF approximation to the single particle potential, i.e. neglecting the momentum dependence of the scalar Σ_s and vector fields Σ_o and Σ_v in Eqs. (6) and (10). The single particle energy is
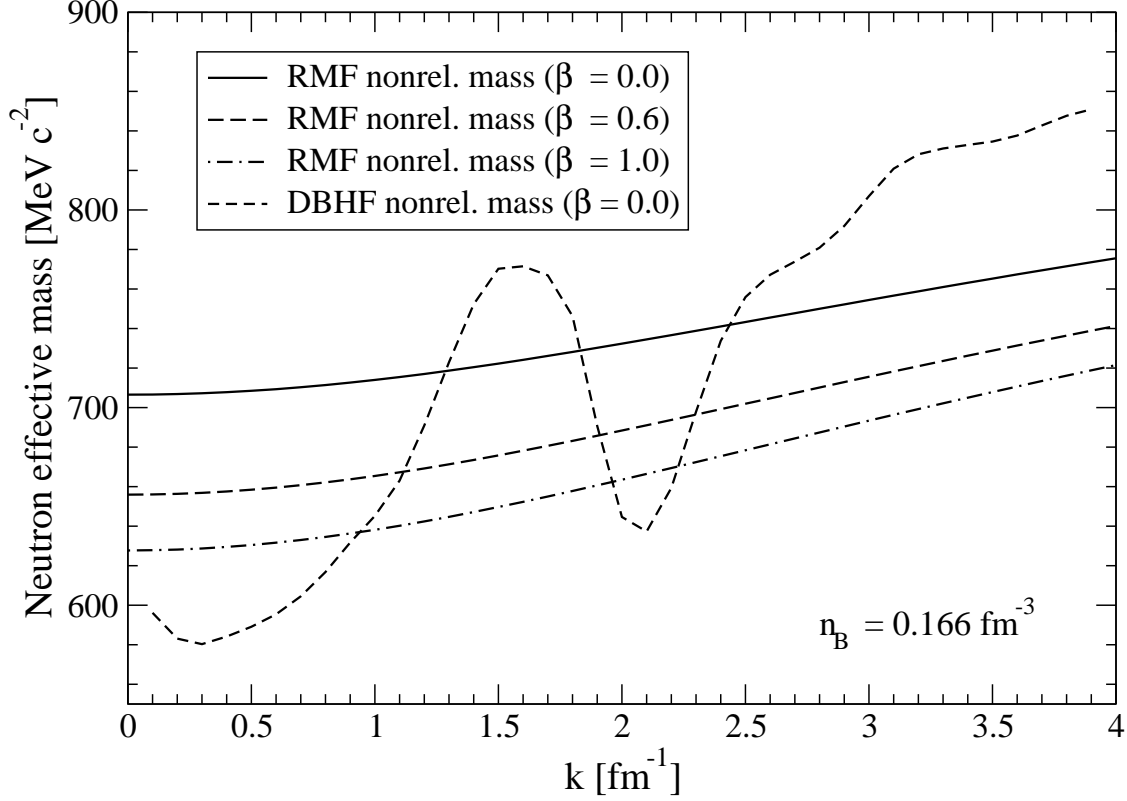
19

FIG. 12: Neutron effective mass obtained in the RMF approximation as a function of the momentum $k = |\mathbf{k}|$ at fixed nuclear density $n_B = 0.166$ fm^{-3}.

now given by

$$E_{RMF} = (1 + \Re\Sigma_{\mathrm{v}}(k_{\mathrm{F}}))\sqrt{|\mathbf{k}|^2 + m_D^{*2}(k_{\mathrm{F}})} + \Re\Sigma_{\mathrm{o}}(k_{\mathrm{F}}). \tag{13}$$

In Fig. 12 this "RMF" nonrelativistic mass is plotted for various values of the asymmetry parameter β at fixed nuclear density $n_B = 0.166$ fm^{-3}. For comparison the full DBHF nonrelativistic mass for symmetric nuclear matter is shown as well. Because of the parabolic momentum dependence of the RMF single particle energy E_{RMF}, the corresponding RMF mass has no bump or peak structure but is a continuously rising function with momentum. The nonrelativistic RMF mass at $k = k_F$ corresponds to the RMF Landau mass [40, 51]. The RMF nonrelativistic mass decreases with increasing asymmetry. In isospin asymmetric matter RMF theory predicts the same proton-neutron mass splitting for the Dirac and the nonrelativistic mass, i.e. $m_{D,n}^* < m_{D,p}^*$ and $m_{NR,n}^* < m_{NR,p}^*$. This behavior is a general feature of the RMF approach [14]. Concerning the Dirac mass full DBHF theory is in agreement with the prediction of RMF theory. However, the mass splitting of the nonrelativistic

mass is reversed due to the momentum dependence of the self-energies, which is neglected in RMF theory.

V.   SUMMARY AND CONCLUSIONS

In summary, we present calculations of isospin symmetric and asymmetric nuclear matter in the DBHF approach based on projection techniques. We compared the momentum, density, and isospin dependence of the relativistic Dirac mass and the nonrelativistic mass. Furthermore, we also investigated these dependencies of the isovector optical potential. Firstly, the nonrelativistic mass derived from the DBHF approach should be based on the Schroedinger equivalent potential (10) [40] to be able to compare it to nonrelativistic approaches. The alternative, to derive it directly from Eq. (7) via the relativistic single particle energy $E = (1 + \Re\Sigma_\mathrm{v})\sqrt{\mathbf{k}^2 + m_D^{*2}} - \Re\Sigma_\mathrm{o}$, contains relativistic corrections to the kinetic energy. Secondly, the nonrelativistic effective mass shows a characteristic peak structure at momenta slightly above the Fermi momentum k_F as it is also seen in nonrelativistic BHF calculations, e.g. [40]. This peak structure reflects the increase of the level density at Fermi momentum $k = k_\mathrm{F}$. In contrast, the Dirac mass is a smooth function of k with a weak momentum dependence. Thirdly, a strong momentum dependence on both effective masses, the nonrelativistic mass and the Dirac mass, is observed. Fourthly, it turns out that the isovector optical potential depends sensitively on density and momentum, but is almost insensitive to the isospin asymmetry. In addition, the empirical isovector potential extracted from proton-nucleus scattering is well reproduced by our calculation. Finally, the controversy between relativistic and nonrelativistic approaches concerning the proton-neutron mass splitting in asymmetric nuclear matter has been resolved. The relativistic Dirac mass shows a proton-neutron mass splitting of $m_{D,n}^* < m_{D,p}^*$, in line with RMF theory. However, the nonrelativistic mass derived from the DBHF approach has a reversed mass splitting $m_{NR,n}^* > m_{NR,p}^*$ which is in agreement with the results from nonrelativistic BHF calculations.

Acknowledgments

[1] J. M. Lattimer, C. J. Pethick, M. Prakash, and P. Haensel, Phys. Rev. Lett. **66**, 2701 (1991).

[2] E. N. E. van Dalen, A. E. L. Dieperink, A. Sedrakian, and R. G. E. Timmermans, Astron. & Astrophys. **360**, 549 (2000)

[3] E. N. E. van Dalen and A. E. L. Dieperink, *Proceedings of the international school of physics Enrico Fermi Course CLIII: Varenna 2002 From Nuclei and their Constituents to Stars*, 169 (2003).

[4] M. Prakash, T. L. Ainsworth, and J. M. Lattimer, Phys. Rev. Lett. **61**, 2518 (1988).

[5] L. Engvik et al., Phys. Rev. Lett. **73**, 2650 (1994).

[6] C. H. Lee, Phys. Rep. **275**, 255 (1996).

[7] S. Kubis and M. Kutschera, Acta Phys. Polon. B **30**, 2747 (1999).

[8] M. Kutschera and J. Niemic, Phys. Rev. C **62**, 025802 (2000).

[9] B. L. Friman and O. V. Maxwell, Astrophys. J. **232**, 541 (1979).

[10] A. E. L. Dieperink, E. N. E. van Dalen, A. Korchin, and R. Timmermans, *Hadrons, Nuclei and Applications; Proceedings of the conference: Bologna 2000 Structure of the Nucleus at the Dawn of the Century*, 293 (2001);

[11] D.G. Yakovlev, A.D. Kaminker, O.Y. Gnedin, and P.Haensel, Phys. Rep. **354**, 1 (2001).

[12] R. G. E. Timmermans, A. Yu. Korchin, E. N. E. van Dalen, and A. E. L. Dieperink, Phys. Rev. C **65**, 064007 (2002).

[13] E. N. E. van Dalen, A. E. L. Dieperink, and J. A. Tjon, Phys. Rev. C **67**, 065807 (2003).

[14] V. Baran, M. Colonna, V. Greco, and M. Di Toro, Phys. Rep. **410**, 335 (2005).

[15] J. Rizzo, M. Colonna, and M. Di Toro, Nucl. Phys. **A732**, 202 (2004).

[16] B.-A. Li, Phys. Rev. C **69**, 064602 (2004).

[17] L.-W. Chen, C.M. Ko, and B.-A. Li, Phys. Rev. Lett. **94**, 032701 (2005).

[18] D.V. Shetty, S.J. Yennello, and G.A. Souliotis, nucl-ex/0505011.

[19] V. S. Uma Maheswari, C. Fuchs, Amand Faessler, L. Sehn, D. Kosov, and Z. Wang, Nucl. Phys. **A628**, 669 (1998).

[20] T. Gaitanos, M. Di Toro, S. Typel, V. Baran, C. Fuchs, V. Greco, and H.H. Wolter, Nucl. Phys. **A732**, 24 (2004).

[21] I. Bombaci and U. Lombardo, Phys. Rev. C **44**, 1892 (1991).

[22] D. Vretenar, T. Nikšić, and P. Ring, Phys. Rev. C **68**, 024310 (2003).

[23] W. Zuo, I. Bombaci, and U. Lombardo, Phys. Rev. C **60**, 024605 (1999).

[24] T. Frick, Kh. Gad, H. Müther, and P. Czerski, Phys. Rev. C **65**, 034321 (2002)

[25] Kh.S.A. Hassaneen and H. Müther, Phys. Rev. C **70**, 054308 (2004) .

[26] W. Zuo, L. G. Cao, B. A. Li, U. Lombardo, and C. W. Shen, Phys.Rev. C **72**, 014005 (2005).

[27] B. Liu, V. Greco,V. Baran, M. Colonna, and M. Di Toro, Phys. Rev. C **65**, 045201 (2002).

[28] E. N. E. van Dalen, C. Fuchs, and A. Faessler, Phys. Rev. Lett. **95**, 022302 (2005).

[29] T. Gross-Boelting, C. Fuchs, and A. Faessler, Nucl. Phys. **A648**, 105 (1999).

[30] E. N. E. van Dalen, C. Fuchs, and A. Faessler, Nucl. Phys. **A744**, 227 (2004).

[31] B. Ter Haar and R. Malfliet, Phys. Rep. **149** 207 (1987).

[32] L. Sehn, C. Fuchs, and A. Faessler, Phys. Rev. C **56**, 216 (1997).

[33] R. Brockmann and R. Machleidt, Phys. Rev. C **42**, 1965 (1990).

[34] E. Schiller and H. Müther, Eur. Phys. J. A **11**, 15 (2001).

[35] G. A. Lalazissis, J. König, and P. Ring, Phys. Rev. C **55**, 540 (1997).

[36] S. Typel, Phys.Rev. C **71**, 064301 (2005).

[37] G.E. Brown, J.H. Gunn, and P. Gould, Nucl. Phys. **46**, 598 (1963).

[38] J. P. Jeukenne, A. Lejeune, and C. Mahaux, Phys. Rep. **25**, 83 (1976).

[39] C. Mahaux, P.F. Bortignon, R.A. Broglia, and C.H. Dasso, Phys. Rep. **120**, 1 (1985).

[40] M. Jaminon and C. Mahaux, Phys. Rev. C **40**, 354 (1989).

[41] H. Müther, (private communication).

[42] M. Kleban, B. Nerlo-Pomorska, J. F. Berger, J. Decharge, M. Girod, and S. Hilaire, Phys. Rev. C **65**, 024309 (2002).

[43] B. Cochet, K. Bennaceur, J. Meyer, P. Bonche, and T. Duguet, Int. J. Mod. Phys. **E13**, 187 (2004).

[44] L.-W. Chen, C.M. Ko, and B.-A. Li, nucl-th/0509009.

[45] J.A. McNeil, J.R. Shepard, and S.J. Wallace, Phys. Rev. C **27**, 2123 (1983).

[46] A.M. Lane, Nucl. Phys. **35**, 676 (1962).

[47] R. Kozack and D.G. Madland, Phys. Rev. C **39**, 1461 (1989); Nucl. Phys. **A509**, 664 (1990).

[48] D. Alonso and F. Sammarruca, Phys. Rev. C **67**, 054301 (2003)

[49] F. Sammarruca, W. Barredo, and P. Krastev, Phys. Rev. C **71**, 064306 (2005).

[50] F. de Jong and H. Lenske, Phys. Rev. C **58**, 890 (1998).

[51] T. Matsui, Nucl. Phys. **A370**, 365 (1981).